

Increased hygroscopicity of Arizona Test Dust seeds by secondary organic aerosol coating from α -pinene ozonolysis

Helmi Keskinen¹⁾, Aki-Matti Kortelainen¹⁾, Antti Jaatinen¹⁾, Pasi Yli-Pirilä¹⁾, Jorma Joutsensaari¹⁾, Sami Romakkaniemi¹⁾⁶⁾, Li-Qing Hao¹⁾, Tiina Torvela²⁾, Pasi Miettinen¹⁾, Annele Virtanen¹⁾, Douglas R. Worsnop¹⁾⁴⁾, Ari Laaksonen¹⁾³⁾ and James N. Smith¹⁾⁵⁾

¹⁾ Department of Applied Physics, University of Eastern Finland, P.O. Box 1627, FI-70211 Kuopio, Finland

²⁾ Department of Environmental Science, University of Eastern Finland, P.O. Box 1627, FI-70211 Kuopio, Finland

³⁾ Finnish Meteorological Institute, P.O. Box 503, FI-00101 Helsinki, Finland

⁴⁾ Aerodyne Research, 45 Manning Road, Billerica, MA 01821, USA

⁵⁾ National Center for Atmospheric Research, P.O. Box 3000, Boulder, CO 80307-3000, USA

⁶⁾ Finnish Meteorological Institute, P.O. Box 1627, FI-70211 Kuopio, Finland

Received 4 Nov. 2013, final version received 23 Apr. 2014, accepted 17 Apr. 2014

Keskinen, H., Kortelainen, A.-M., Jaatinen, A., Yli-Pirilä, P., Joutsensaari, J., Romakkaniemi, S., Hao, L. Q., Torvela, T., Miettinen, P., Virtanen, A., Worsnop, D. R., Laaksonen, A. & Smith, J. N. 2014: Increased hygroscopicity of Arizona Test Dust seeds by secondary organic aerosol coating from α -pinene ozonolysis. *Boreal Env. Res.* 19 (suppl. B): 182–190.

Organic compounds can enhance the hygroscopic properties of insoluble dust particles and thereby affect their cloud condensation nuclei activity in the atmosphere. In this study, Arizona Test Dust (ATD) particles were exposed to oxidized organic vapors from the ozonolysis of α -pinene in a laboratory chamber. The particle size-dependent morphology, inorganic and organic composition and hygroscopic properties were studied. The dust consisted of particles with a range of morphologies from spherical to geometrical, with a size range from 50 nm to 1 μ m. Exposure to oxidized organics resulted in a separate mode of secondary organic aerosol (SOA) particles with size ranging below 100 nm and a well-mixed ATD + SOA mode at larger sizes. The O:C mole ratio for the organics produced from α -pinene ozonolysis was stable at 0.4 ± 0.05 in all experiments. The results showed that the hygroscopicities of the ATD particles with a diameter of 100–150 nm were enhanced by a factor of four with the addition of SOA, corresponding to a particulate organic volume fraction of ~ 0.6 and an average κ of 0.09.

Introduction

Atmospheric particulate matter contains dust and organic matter from natural emission sources such as deserts and forests. Several laboratory and field investigations have been performed

to elucidate the role that organic aerosol (e.g., Jimenez *et al.* 2009) and dust (Kumar *et al.* 2011) play separately as cloud condensation nuclei (CCN) in the atmosphere. However, understanding the combined role of dust and organics in aerosol–cloud interactions is needed

in order to determine their present and future impacts on climate (IPCC 2007). This may be particularly important for boreal-forest regions, which are characterized by high levels of secondary organic aerosol (SOA) precursor gases such as monoterpenes (Hakola *et al.* 2003), clean conditions with few anthropogenic sources, and, in some locales, incursions of long-range-transported dust. Examples of the latter include trans-Pacific dust events that originate in the Gobi and Takla Makan deserts in Asia and impact the Pacific Northwest region of North America (e.g. Leaitch *et al.* 2003). Dust from these and other Asian deserts is very likely to be occasionally transported to Siberian forests as well. Monoterpenes are of course emitted from other types of biomes as well, some of which are located in close proximity to deserts.

By measuring hygroscopicity we gain information on aerosol cloud-droplet activation properties as well as on certain physico-chemical properties such as composition (Petters and Kreidenweis 2007, Keskinen *et al.* 2013). Inorganic mineral and dust particles are not very hygroscopic but they still have ability to act as cloud condensation nuclei (e.g. Vlasenko *et al.* 2005, 2006, Herich *et al.* 2009, Kumar *et al.* 2009, 2011, Koehler *et al.* 2009). A recent study by Kumar *et al.* (2011) focused on the CCN activity of fresh dust particles from multiple sources (e.g., Arizona and Sahara). Their major finding was that freshly-emitted dust and mineral aerosols could act as CCN through the effects of water adsorption alone. Specifically, they showed that 100 nm dust particles can exhibit comparable hygroscopicity to organic species or to a particle with an ammonium sulfate (AS) volume fraction of 0.1. Besides salt, atmospheric particles contain organics (Jimenez *et al.*, 2009, Halquist *et al.* 2009). SOA itself, e.g., that formed by α -pinene oxidation, is also known to be hygroscopic (Jimenez *et al.* 2009, Saathof *et al.* 2003). In the atmosphere, organic matter can heterogeneously coat solid particles and thus affect the hygroscopic properties and cloud droplet activation of these particles. For example, the hygroscopicity of nanoscale soot agglomerates increases by the uptake of organics, up to the hygroscopicity of pure SOA (Saathof *et al.* 2003). In addition, Hatch *et al.* (2008) and

Gierlus *et al.* (2011) observed an increase in the hygroscopicity of pure calcite nanoparticles by organic acids. Though the impact of SOA-coated dust on cold cloud formation has been studied (Koehler *et al.* 2010), to our knowledge laboratory studies focusing on its impacts on warm cloud formation have not yet been performed.

In this study, we measured the hygroscopicity of well-defined Arizona Test Dust (ATD) seed particles exposed to SOA from the ozonolysis of α -pinene in the Kuopio aerosol research chamber (Hao *et al.* 2011). We report SOA coating amount and its effect on ATD hygroscopicity. The overarching scientific goal of this study is to improve understanding of the interactions between suspended dust and condensable organic compounds, and the role that the uptake of organics may play in warm cloud formation in regions such as the boreal forest. In addition to studying the hygroscopicity of SOA-coated dust, we will also determine the degree to which particulate mass increases as a result. This increased growth rate has implications for CCN activation, since larger particles are more effective condensation nuclei. In addition, dust particles inside cloud droplets may cause immersion freezing if the droplets become cold enough. If a SOA coating were to increase the hygroscopicity of a dust particle, it is more likely that it would form a cloud droplet. In this manner, a SOA coating on dust may increase the probability of the occurrence of immersion freezing.

Experimental methods

We used the Kuopio 6 m³ aerosol chamber to coat the ATD nanoparticles with SOA formed from α -pinene ozonolysis. The ATD particles were generated from an aqueous suspension by a collision-type atomizer (model 3076, TSI, Inc., USA). The solid content in the water suspension of ATD (0–3 μ m, Powder Technology, Inc., USA) was set to 0.1 wt%. The produced aerosol was fed into a diffusion drier consisting of a porous tube surrounded by silica gel, resulting in relative humidity (RH) below 5%.

The samples for electron microscopy were collected on perforated carbon–copper grids (300 Mesh Cu, Agar Scientific, UK) by depositing

drops of diluted suspension (0.005 wt%) directly on the grid, and drying under atmospheric conditions. In separate investigations, we produced atomized aerosol as described in the previous paragraph and collected those particles on a grid for comparison with the particles created from droplets. The grids containing the atomized particles captured far fewer particles, so we chose the droplet method for spectroscopic analysis. However, in comparing individual particles created by both techniques we could find no significant differences in either their morphology or composition.

The morphology and crystallinity of the ATD particles were studied by transmission electron microscopy (TEM) (model JEM 2100F, JEOL Ltd., Japan) operated at 200 kV acceleration voltage. The primary particle size was estimated from TEM micrographs using ImageJ software (National Institutes of Health, USA). The elemental composition of the particles was analysed using energy dispersive X-ray spectroscopy (EDS) in spot analysis mode. In order to spatially resolve the elemental composition of particles from that of the background, a spectral image consisting of an elemental spectrum obtained for a $725 \text{ nm} \times 725 \text{ nm}$ region with a $2.8 \text{ nm pixel}^{-1}$ resolution was acquired from a representative particle. Fifty frames with 0.5 ms dwell time were collected in scanning mode of TEM. Two principal components were resolved from the spectral image using the multivariate statistical analysis tool of the EDS analyser software (NORAN System 7, Thermo Scientific, USA). By using the principal components, joint spectra of the particle and the background were constructed.

Before each chamber experiment, the aerosol chamber was flushed and filled with pure filtered, dry air. Next, the ATD particles were introduced into the chamber and diluted achieving the desired concentration ($\sim 10^4 \text{ cm}^{-3}$). Following this, $2 \mu\text{l}$ of α -pinene was injected into the chamber, resulting in a measured gas phase concentration of $33 \pm 1 \text{ ppb}$. After 15 min mixing time, ozone enriched air (1.5 ppm at 30 l min^{-1}) was introduced into the chamber to achieve ozone concentration of $50 \pm 10 \text{ ppb}$ to initiate oxidation. Ozone was generated by a UV lamp O_3 generator. About 40% of α -pinene was reacted in 30 minutes after the ozone addition based on

the volatile organic compounds (VOC) analysis. Following this, all flows into the chamber were turned off and chamber volume was slowly decreased by the flow required by the instruments (10.4 l min^{-1}). The experiments were performed for about four hours, which includes the time required for stabilizing the seed particle concentration. In all experiments, NO_x was $3 \pm 0.5 \text{ ppb}$ (i.e. low NO_x conditions), temperature was $25 \pm 2 \text{ }^\circ\text{C}$, and RH was $5\% \pm 2\%$.

VOCs were collected onto Tenax TA adsorbent (mesh 60/80, Supelco Analytical, USA) for 10 minutes with an air flow through the sample tube of 200 ml min^{-1} . The trapped compounds were analyzed with a thermal desorption unit (model ATD400 Automatic Thermal Desorption System, Perkin-Elmer Inc., USA) coupled to a gas chromatograph-mass spectrometer (models GC 6890 and MSD 5973, Hewlett Packard Corp., USA). The compounds were identified by comparing their mass spectra with those in the Wiley 275.L mass spectral library and with pure standards. Details on the analysis of VOCs can be found elsewhere (Vuorinen *et al.* 2004).

During the experiment, the particle size distribution was monitored by a scanning mobility particle sizer (SMPS) consisting of a model 3081 differential mobility analyzer and model 3785 condensation particle counter (TSI, Inc., USA). Aerosol number concentration was also measured with a condensation particle counter (CPC, model 3025, TSI, Inc., USA). The SMPS measurements covered the mobility diameter range of 9–370 nm. Real-time aerosol chemical composition over the vacuum aerodynamic diameter range from 50 to 1000 nm was measured by Aerodyne High Resolution Time-Of-Flight Aerosol Mass Spectrometer (HR-TOF-AMS, Jayne *et al.* 2000, DeCarlo *et al.* 2006) using the standard $600 \text{ }^\circ\text{C}$ vaporizer temperature. Sulphate, organics, ammonium and nitrate mass loadings were determined from the mass spectra, and O:C ratios were derived using the procedure of Aiken *et al.* (2008). Size-resolved CCN activity was measured using a CCN counter (model CCN-100, Droplet Measurements Technologies, USA). The CCN counter was operated using Scanning Mobility CCN Analysis developed by Moore and Nenes (2009), covering the dry particle diameter range from 30 to 200 nm.

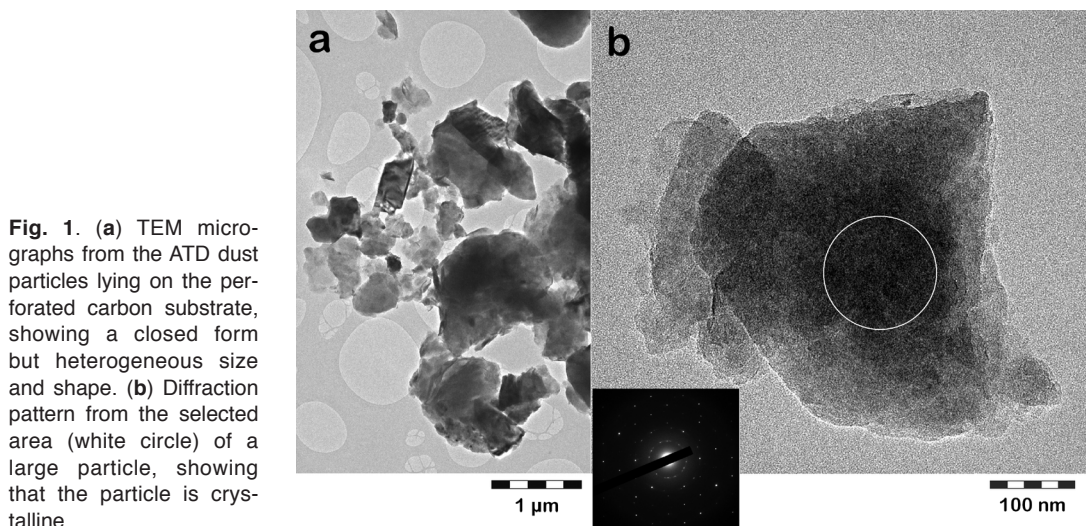


Fig. 1. (a) TEM micrographs from the ATD dust particles lying on the perforated carbon substrate, showing a closed form but heterogeneous size and shape. (b) Diffraction pattern from the selected area (white circle) of a large particle, showing that the particle is crystalline.

In this study, hygroscopicity is represented from CCN measurements using the κ -Köhler theory (Petters and Kreidenweis 2007), recognizing that a number of assumptions are made in applying Köhler theory to cloud droplet activation (Seinfeld and Pandis 2006). In spite of these assumptions, κ -Köhler theory is widely used both in reporting aerosol hygroscopicity measurements and also in the modelling of aerosol properties in large scale models. All references in this manuscript regarding hygroscopicity refer directly to κ_{CCN} defined as follows:

$$\kappa_{\text{CCN}} = \frac{4 \left(\frac{4\sigma_w M_w}{RT\rho_w} \right)}{27d_{\text{dry}}^3 \ln^2 S_c} - 1, \quad (1)$$

where σ_w is the water surface tension, M_w is the molecular weight of the water, R is the ideal gas constant, T is the temperature (K), ρ_w is the density of the liquid water, d_{dry} is the dry diameter of particles selected for analysis, and S_c is the critical supersaturation for each dry diameter. The volume fraction of organics (ε_o) was derived from CCN measurements by assuming a “two-component” particle (Keskinen *et al.* 2013) consisting of organics (o) and ATD (d):

$$\varepsilon_o = \frac{\kappa - \kappa_d}{\kappa_o - \kappa_d}, \quad (2)$$

where κ is the combined overall (measured) hygroscopicity, κ_d is the hygroscopicity for dust

and κ_o for organic compounds. In our calculation we used the measured κ_d and the κ_o for organics based on the AMS-measured oxidation state (Massoli *et al.* 2010).

For comparison, we also determined an average organic volume fraction (f_{ov}) from AMS results and volume size distributions measured with the SMPS. f_{ov} was determined as a ratio of AMS organic volume (V_o) and SMPS total volume (V_{tot}), i.e. $f_{\text{ov}} = V_o/V_{\text{tot}}$. The density of 1.4 (α -pinene ozonolysis product) was used for the AMS organic volume calculation (Kostenidou 2007). Note that the determination of particle volume from the number size distribution is not very accurate, especially for large particles due to low number concentrations, and thus there may be higher uncertainties associated with f_{ov} .

Results and discussion

The uncoated ATD particles had typically diverse shapes from spheres to polygon symmetries (Fig. 1a). The individual particle size measured from TEM-micrographs varied from 50 nm to approximately 1 μm (see for example Figs. 1b and 2a). In addition, the particles were found crystalline (Fig. 1b). The ATD particles were mainly composed of Si, O, and C, determined using the EDS spot analysis. However, trace amounts (mass fraction below 2%) of Al, Fe, Ca, K and Mg were also detected in various

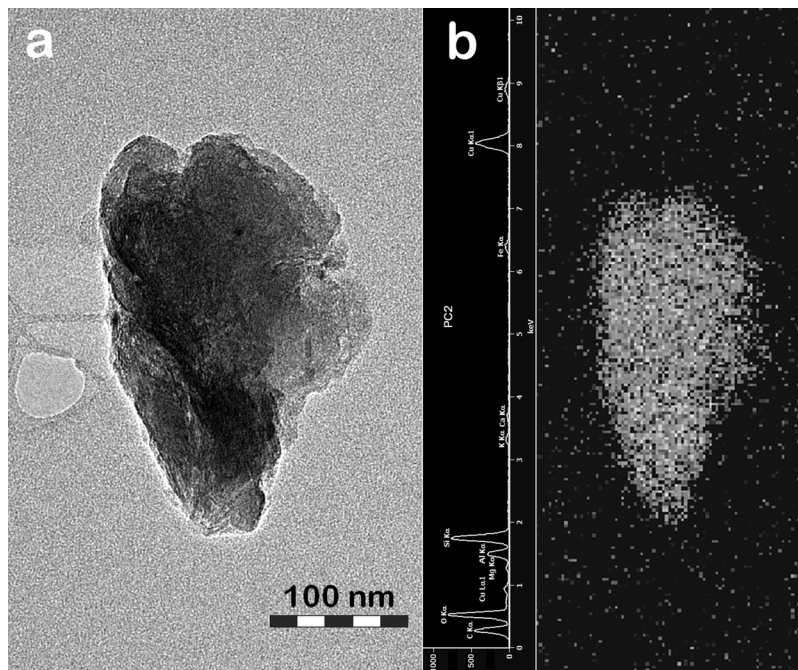


Fig. 2. (a) TEM bright field image of an ATD particle. (b) High intensity pixels show a reconstruction of the second principal component (PC2) of multivariate analysis on the EDS map of the particle area and background. The combined element spectrum is shown on the left. According to the analysis, the particle is composed of C, O, Al, Si, K, Ca and Fe. The Cu peaks at approximately 0.9, 8, and 9 keV in the particle spectra were due to background scattering from the sample grid.

particles. A typical example of the composition is shown in Fig. 2b (left-hand side) showing the second principal component (PC2) spectrum calculated from the spectral image of the particle in Fig. 2a. The high intensity pixels in Fig. 2b show the similar regions compared to PC2 spectrum. As with the various spot analyses, Si, O, C, Al, Fe, Ca, K, Mg and Cu were detected. By experience and the first principal component of spectral image (PC1), it was known that incidences of Cu were from background scattering of the substrate grid. The other elements of PC1 were C, O, Cr, and Si, and they were distributed evenly amongst background and particles. Although Ti and Na were not found, the detected elements corresponded with the composition measured by Vlasenko *et al.* (2005), and with that provided by the supplier of the ATD: SiO₂, Al₂O₃, Fe₂O₃, Na₂O, CaO, MgO, TiO₂ and K₂O.

Before the SOA formation, a bimodal distribution was observed for the pure ATD with the first mode geometric mean diameter (GMD) of 26 nm and second mode GMD of 114 nm (Fig. 3b). A similar bimodal distribution for the wet-atomized ATD was observed by Gustavsson *et al.* (2005), who speculated that water-soluble species in the mineral dust collected from the ATD form

the first mode, and that the second mode consists of the actual mineral dust. The water-soluble mode composition of the ATD was analysed by Vlasenko *et al.* (2005), who found that this mode comprises about 2% of the particulate mass and consists mostly of sulphates. However, as the mass of these first-mode particles is substantially low, this fraction is likely not observed by the AMS due to the detection limits of the method (further discussion of this is provided below).

With α -pinene ozonolysis the particle number size distribution changed dramatically (Fig. 3). The total number concentration increased from 8000 to 12 600 cm⁻³ after the SOA addition, evidence that new-particle formation occurred. Interestingly, sub-20 nm diameter particles were not observed after α -pinene ozonolysis (Fig. 3a), even though the clear increase in total number concentration provides evidence that new particles were formed. We hypothesize that newly-formed particles grew rapidly to a diameter of ~30 nm and where therefore not detected by the SMPS during this period. This phenomenon of a very rapid initial growth of newly-formed particles from α -pinene ozonolysis was also observed by Winkler *et al.* (2012). In addition to forming new particles, low-volatility organic compounds

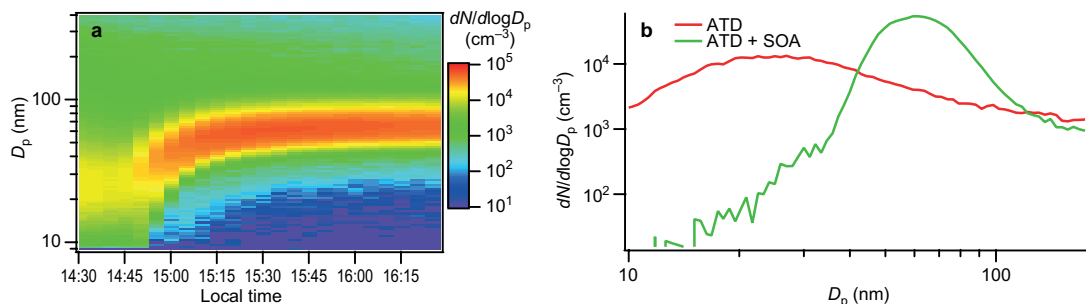


Fig. 3. (a) Size distribution evolution from pure ATD to ATD + SOA. (b) The size distribution before (14:40, red line) and after (15:30, green line) SOA formation.

condensed onto the smaller-mode ATD particles (water soluble salts), reaching a geometric mean diameter of ~ 60 nm, as well as onto the larger-mode ATD particles (> 100 nm). This resulted in an external mixture of SOA-coated salts, SOA-coated mineral dust and pure organic particles. Note that the number concentration did not increase in the size range above 100 nm, and thus a great majority of these particles were very likely SOA-coated dust.

Measurements of mass-averaged chemical composition by HR-TOF-AMS during SOA-exposure showed that organics dominated the particle composition following α -pinene ozonolysis (Fig. 4). However, it is important to note that the instrument cannot detect dust minerals, nor can it detect particles smaller than ~ 30 nm in diameter. Particles contained small amounts of water-soluble salts such as sulphates and nitrates (Fig. 4), consistent with those compounds being primarily associated with the smaller water-soluble mode. The O:C ratio of the condensed SOA material derived from HR-TOF-AMS measurements was 0.4 ± 0.1 .

As speculated, the ATD particles below 120 nm in diameter most likely contained water-soluble salts (e.g. sulphates) from dust itself, as the measured hygroscopicities were higher than the value of 0.025 observed by Kumar and colleagues for dry-synthesized ATD. The hygroscopicity of SOA-coated dust particles was roughly four times higher than that of dry-synthesized dust particles at diameters greater than 80 nm, with a constant κ of 0.09 for 100–150 nm diameter particles (Fig. 5a). Thus, the coating had a remarkable effect on the ability of dust particles to act as cloud condensation nuclei. Below

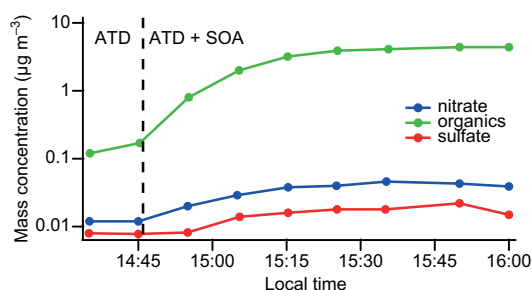


Fig. 4. The time evolution of organics, nitrate, and sulphate mass concentrations during the experiment, as measured by the HR-TOF-AMS.

100 nm, the particles included only organics and possible impurities in ATD, e.g. salts (Fig. 5b). At this size range, the hygroscopicities of individual compounds were similar (Fig. 5a), thus providing a non-unique solution to analysis of composition by the ZSR technique. For the size range from 100 to 150 nm, the value of f_{ov} was 0.6 ± 0.07 . For comparison, the average organic volume fraction calculated from SMPS volume size distributions and AMS organics was 0.56 ± 0.25 , which supports our hygroscopicity-derived results.

A simple calculation can provide an estimate of how long would it take in the boreal forest atmosphere to obtain an organic coating corresponding to a f_{ov} of 0.6. Observations from the Finnish boreal forest show that diameter growth rates associated with new particle formation typically range from 1 to 10 nm h⁻¹ (Kulmala *et al.* 2004). If we consider a dust particle with diameter of 150 nm, a characteristic diameter based on our observations, then the diameter after growth by organics, that is, associated with a f_{ov} of 0.6, would be 204 nm. Consequently, a growth rate

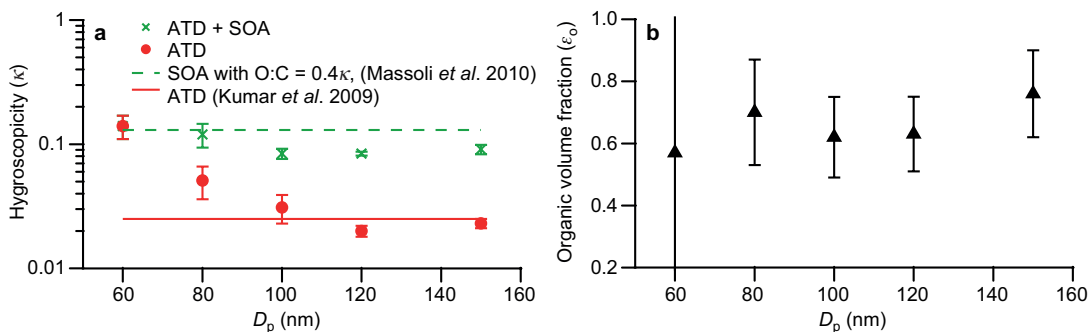


Fig. 5. (a) Hygroscopicity, κ , measured by the CCN counter versus particle size for pure ATD and ATD exposed to α -pinene oxidation products. The lines represent the values of pure ATD-dust (Kumar *et al.* 2009), and α -pinene oxidation products with O:C ratio of 0.4 (Massoli *et al.* 2010). (b) Organic volume fraction, ϵ_o (Eq. 2) for the ATD + SOA particles in the particles evaluated from the measured hygroscopicities.

of 1 nm h^{-1} corresponds to a time of 50 hours to grow to this diameter; a 10 nm h^{-1} growth rate would correspond to about five hours of growth time.

Conclusions

Arizona Test Dust (ATD) seeds were exposed to the gas-phase products from the ozonolysis of α -pinene. The particle size-dependent inorganic and organic composition and hygroscopic properties were measured. Dust consisted of nanoparticles of various shapes, and of diameter range from 50 nm to $1 \mu\text{m}$. Exposure of these particles to the reaction products of α -pinene ozonolysis resulted in an external mixture consisting of SOA and SOA-coated ATD particles. The SOA had a measured O:C ratio of 0.4 ± 0.1 . The pure dust had substantially higher hygroscopicities below 100 nm because soluble salts (e.g. sulphates) are expected to dominate ATD composition over that size range. For the ATD + SOA particles with diameters from 100 to 150 nm, hygroscopicities were enhanced by a factor of four as compared with pure ATD with an observed SOA fraction of ~ 0.6 and average κ of 0.09. These observations confirm that insoluble particulate matter such as dust can act as a condensation or deposition surface for the low-volatility products of VOC oxidation in atmosphere. The resulting SOA can remarkably enhance the dust hygroscopicity and thereby increase the ability of the particle to act as a CCN.

Acknowledgements: This work was supported by the Academy of Finland Centre of Excellence (grant no. 1118615 and decision numbers 138951, 267514, 118230, 252908), the strategic funding of the University of Eastern Finland, the Kone and Saastamoinen Foundations, and the “Cryosphere–atmosphere interactions in a changing Arctic climate” (CRAICC) research initiative. The National Centre for Atmospheric Research is sponsored by the U. S. National Science Foundation. JNS acknowledges funding from the US Department of Energy.

References

- Aiken A.C., Decarlo P.F., Kroll J.H., Worsnop D.R., Huffman J.A., Docherty K.S., Ulbrich I.M., Mohr C., Kimmel J.R., Sueper D., Sun Y., Zhang Q., Trimborn A., Northway M., Ziemann P.J., Canagaratna M., Onasch T.B., Alfarra M.R., Prevot A.S.H., Dommen J., Duplissy J., Metzger A., Baltensperger U. & Jimenez J.L. 2008. O/C and OM/OC ratios of primary, secondary, and ambient organic aerosols with high-resolution time-of-flight aerosol mass spectrometry. *Environ. Sci. Technol.* 42: 4478–4485.
- DeCarlo P.F., Kimmel J.R., Trimborn A., Northway M.J., Jayne J.T., Aiken A.C., Gonin M., Fuhrer K., Horvath T., Docherty K., Worsnop D.R. & Jimenez J.L. 2008. Field-deployable, high-resolution, time-of-flight aerosol mass spectrometer. *Anal. Chem.* 78: 8281–8289.
- Gierlus K.M., Laskina O., Abernathy T.L. & Grassian V.H. 2012. Laboratory study of the effect of oxalic acid on the cloud condensation nuclei activity of mineral dust aerosol. *Atmos. Environ.* 46: 125–130.
- Gustafsson R.J., Orlov A., Badger C.L., Griffiths P.T., Cox R.A. & Lambert R.M. 2005. A comprehensive evaluation of water uptake on atmospherically relevant mineral surfaces: DRIFT spectroscopy, thermogravimetric analysis and aerosol growth measurements. *Atmos. Chem. Phys.* 5: 3415–3421.
- Hakola H., Tarvainen V., Laurila T., Hiltunen V., Hellen H. &

- Keronen P. 2003. Seasonal variation of VOC concentrations above a boreal coniferous forest. *Atmos. Environ.* 37: 1623–1634.
- Hallquist M., Wenger J.C., Baltensperger U., Rudich Y., Simpson D., Claeys M., Dommen J., Donahue N.M., George C., Goldstein A.H., Hamilton J.F., Herrmann H., Hoffmann T., Iinuma Y., Jang M., Jenkin M., Jimenez J.L., Kiendler-Scharr A., Maenhaut W., McFiggans G., Mentel Th.F., Monod A., Prévôt A.S.H., Seinfeld J.H., Surratt J.D., Szmigielski R. & Wildt J. 2009. The formation, properties and impact of secondary organic aerosol: current and emerging issues. *Atmos. Chem. Phys.* 9: 5155–5236.
- Hao L.Q., Romakkaniemi S., Yli-Pirilä P., Joutsensaari J., Kortelainen A., Kroll J.H., Miettinen P., Vaattovaara P., Tiitta P., Jaatinen A., Kajos M.K., Holopainen J.K., Heijari J., Rinne J., Kulmala M., Worsnop D.R., Smith J.N. & Laaksonen A. 2011. Mass yields of secondary organic aerosols from the oxidation of α -pinene and real plant emissions. *Atmos. Chem. Phys.* 11: 1367–1378.
- Hatch C.D., Gierlus K.M., Schuttlefield J.D. & Grassian V.H. 2008. Water adsorption and cloud condensation nuclei activity of calcite and calcite coated with model humic and fulvic acids. *Atmos. Environ.* 42: 5672–5684.
- Herich H., Tritscher T., Wiacek A., Gysel M., Weingartner E., Lohmann U., Baltensperger U. & Cziczo D.J. 2009. Water uptake of clay and desert dust aerosol particles at sub- and supersaturated water vapor conditions. *Phys. Chem. Chem. Phys.* 11: 7804–7809.
- IPCC 2007. *Climate change 2007: the physical science basis*. Contribution of Working Group I to the Fourth Assessment Report of the Intergovernmental Panel on Climate Change, Cambridge University Press, United Kingdom.
- Jayne J.T., Leard D.C., Zhang X., Davidovits P., Smith K.A., Kolb C.E. & Worsnop D.R. 2000. Development of an Aerosol Mass Spectrometer for size and composition analysis of submicron particles. *Aerosol Sci. Technol.* 33: 49–70.
- Jimenez J.L., Canagaratna M.R., Donahue N.M., Prevot A.S.H., Zhang Q., Kroll J.H., DeCarlo P.F., Allan J.D., Coe H., Ng N.L., Aiken A.C., Docherty K.S., Ulbrich I.M., Grieshop A.P., Robinson A.L., Duplissy J., Smith J.D., Wilson K.R., Lanz V.A., Hueglin C., Sun Y.L., Tian J., Laaksonen A., Raatikainen T., Rautiainen J., Vaattovaara P., Ehn M., Kulmala M., Tomlinson J.M., Collins D.R., Cubison M.J., Dunlea E.J., Huffman J.A., Onasch T.B., Alfarra M.R., Williams P.I., Bower K., Kondo Y., Schneider J., Drewnick F., Borrmann S., Weimer S., Demerjian K., Salcedo D., Cottrell L., Griffin R., Takami A., Miyoshi T., Hatakeyama S., Shimono A., Sun J.Y., Zhang Y.M., Dzepina K., Kimmel J.R., Sueper D., Jayne J.T., Herndon S.C., Trimborn A.M., Williams L.R., Wood E.C., Middlebrook A.M., Kolb C.E., Baltensperger U. & Worsnop D.R. 2009. Evolution of organic aerosols in the atmosphere. *Science* 326: 1525–1529.
- Keskinen H., Virtanen A., Joutsensaari J., Tsagkogeorgas G., Duplissy J., Schobesberger S., Gysel M., Riccobono F., Slowik J.G., Bianchi F., Yli-Juuti T., Lehtipalo K., Rondo L., Breitenlechner M., Kupc A., Almeida J., Amorim A., Dunne E.M., Downard A.J., Ehrhart S., Franchin A., Kajos M.K., Kirkby J., Kürten A., Nieminen T., Makhmutov V., Mathot S., Miettinen P., Onnela A., Petäjä T., Praplan A., Santos F.D., Schallhart S., Sipilä M., Stozhkov Y., Tomé A., Vaattovaara P., Wimmer D., Prevot A., Dommen J., Donahue N.M., Flagan R.C., Weingartner E., Viisanen Y., Riipinen I., Hansel A., Curtius J., Kulmala M., Worsnop D.R., Baltensperger U., Wex H., Stratmann F. & Laaksonen A. 2013. Evolution of particle composition in CLOUD nucleation experiments. *Atmos. Chem. Phys.* 13: 5587–5600.
- Koehler K.A., Kreidenweis S.M., DeMott P.J., Petters M.D., Prenni A.J. & Carrico C.M. 2009. Hygroscopicity and cloud droplet activation of mineral dust aerosol. *Geophys. Res. Lett.* 36, L08805, doi:10.1029/2009GL037348.
- Koehler K.A., Kreidenweis S.M., DeMott P.J., Petters M.D., Prenni A.J. & Mohler O. 2010. Laboratory investigations of the impact of mineral dust aerosol on cold cloud formation. *Atmos. Chem. Phys.* 10: 11955–11968.
- Kostenidou E., Pathak R.K. & Pandis S.N. 2007. An algorithm for the calculation of secondary organic aerosol density combining AMS and SMPS data. *Aerosol Sci. Technol.* 41: 1002–1010.
- Kumar P., Nenes A. & Sokolik I. N. 2009. Importance of adsorption for CCN activity and hygroscopic properties of mineral dust aerosol. *Geophys. Res. Lett.* 36, L24804, doi:10.1029/2009GL040827.
- Kumar P., Sokolik I.N. & Nenes A. 2011. Measurements of cloud condensation nuclei activity and droplet activation kinetics of fresh unprocessed regional dust samples and minerals. *Atmos. Chem. Phys.* 11: 3527–3541.
- Kulmala M., Vehkamäki H., Petäjä T., Dal Maso M., Lauri A., Kerminen V.-M., Birmili W. & McMurry P. 2004. Formation and growth rates of ultrafine atmospheric particles: a review of observations. *J. Aerosol Sci.* 35: 143–176.
- Leitch W.R., Macdonald A.M., Anlauf K.G., Liu P.S.K., Toom-Sauntry D., Li S.M., Liggio J., Hayden K., Wasey M.A., Russell L.M., Takahama S., Liu S., van Donkelaar A., Duck T., Martin R.V., Zhang Q., Sun Y., McKendry I., Shantz N.C. & Cubison M. 2009. Evidence for Asian dust effects from aerosol plume measurements during INTEX-B 2006 near Whistler, BC. *Atmos. Chem. Phys.* 9: 3523–3546.
- Massoli P., Lambe A.T., Ahern A.T., Williams L.R., Ehn M., Mikkilä J., Canagaratna M.R., Brune W.H., Onasch T.B., Jayne J.T., Petäjä T., Kulmala M., Laaksonen A., Kolb C.E., Davidovits P. & Worsnop D.R. 2010. Relationship between aerosol oxidation level and hygroscopic properties of laboratory generated secondary organic aerosol (SOA) particles. *Geophys. Res. Lett.* 24, L24801, doi:10.1029/2010GL046687.
- Moore R., Nenes A. & Medina J. 2010. Scanning mobility CCN analysis — a method for fast measurements of size resolved CCN distributions and activation kinetics. *Aerosol Sci. Technol.* 44: 861–871.
- Petters M.D. & Kreidenweis S.M. 2007. A single parameter representation of hygroscopicity growth and cloud condensation nucleus activity. *Atmos. Chem. Phys.* 7: 1961–1971.

- Saathoff H., Naumann K.H., Schnaiter M., Schock W., Mohler O., Schurath U., Weingartner E., Gysel M. & Baltensperger U. 2003. Coating of soot and $(\text{NH}_4)_2\text{SO}_4$ particles by ozonolysis products of α -pinene. *J. Aerosol Sci.* 34: 1297–1321.
- Seinfeld J.H. & Pandis S.N. 2006. *Atmospheric chemistry and physics: from air pollution to climate change*, 2nd ed. John Wiley and Sons, New York.
- Vlasenko A., Sjögren S., Weingartner E., Gäggeler H.W. & Ammann M. 2005. Generation of submicron Arizona test dust aerosol: chemical and hygroscopic properties. *Aerosol Sci. Technol.* 39: 452–460.
- Vlasenko A., Sjogren S., Weingartner E., Stemmler K., Gäggeler H.W. & Ammann M. 2006. Effect of humidity on nitric acid uptake to mineral dust aerosol particles. *Atmos. Chem. Phys.* 6: 2147–2160.
- Vuorinen T., Nerg A.M., Ibrahim M.A., Reddy G.V.P. & Holopainen J.K. 2004. Emission of *Plutella xylostella*-induced compounds from cabbages grown at elevated CO_2 and orientation behavior of the natural enemies. *Plant Physiol.* 135: 1984–1992.
- Winkler P.M., Ortega J., Karl T., Cappellin L., Friedli H.R., Barsanti K., McMurry P.H. & Smith J.N. 2012. Identification of the biogenic compounds responsible for size-dependent nanoparticle growth. *Geophys. Res. Lett.* 39, L20815, doi:10.1029/2012GL053253.